PERGAMON

International Journal of Plasticity 20 (2004) 543–560

INTERNATIONAL JOURNAL OF Plasticity

www.elsevier.com/locate/ijplas

Micron-resolution 3-D measurement of local orientations near a grain-boundary in plane-strained aluminum using X-ray microbeams

B.C. Larson[a,*], Wenge Yang[a], J.Z. Tischler[a], G.E. Ice[b], J.D. Budai[a], W. Liu[b], H. Weiland[c]

[a]*Oak Ridge National Laboratory, Condensed Matter Sciences Division, PO Box 2008, Oak Ridge, TN 37831-6030, USA*

[b]*Oak Ridge National Laboratory, Metals and Ceramics Division, PO Box 2008, Oak Ridge, TN 37831-6118, USA*

[c]*Alcoa Technical Center, Alcoa Center, PA 15069, USA*

Received in final revised form 2 June 2003

Abstract

X-ray microbeams have been used to perform nondestructive measurements of the local orientations and microstructure in single-crystal and grain-boundary regions in a columnar Al (0.2 wt.% Mg) tri-crystal deformed 20% in plane-strain. The measurements were made using a recently developed differential-aperture X-ray microscopy (DAXM) technique providing high angular resolution determinations of local orientations with micron 3-D spatial resolution using focused microbeams. The X-ray microbeam technique is described, three-dimensional spatially resolved pole-figures and lattice rotation distributions in single-crystal and grain-boundary regions are presented, and the potential of micron resolution 3-D X-ray structural microscopy for plastic deformation investigations is discussed.
© 2003 Elsevier Ltd. All rights reserved.

Keywords: Deformation; Aluminum; Microbeam; X-ray; Diffraction

* Corresponding author. Tel.: +1-865-574-5506; fax: +1-865-574-414.
E-mail address: larsonbc@ornl.gov (B.C. Larson).

0749-6419/$ - see front matter © 2003 Elsevier Ltd. All rights reserved.
doi:10.1016/S0749-6419(03)00101-3

1. Introduction

Investigations of plastic deformation in metals have accumulated a wealth of detailed microscopic and macroscopic information on the deformation process. Comprehensive transmission electron microscopy (TEM) studies (Hughes and Hansen, 1997; Liu, 1995), electron backscattering orientation imaging microscopy (OIM) (Field, 1997; Sun et al., 2000; Adams et al., 1993; Lassen, 1996), deformation pole-figure and orientation-distribution analysis and simulation (Panchanadeeswaran et al., 1996; Bertram et al., 1997; Nakamachi et al., 2002; Lopes et al., 2003; Maudlin et al., 2003), theoretical analyses (Needleman, 2000; Kubin et al., 1998; Hansen and Huang, 1998; Hansen et al., 2001; El-Azab, 2000; Hirsch and Roberts, 1995; Hähner and Zaiser, 1997; Fleck and Hutchinson, 1997; Gao et al., 1999; Huang et al., 2000, Richmond and Alexandrov, 2000), and increasingly powerful computer simulations (Devincre et al., 2001; Cleri et al., 1997; Bulatov et al., 1998; Radhakrishnan et al., 1998; Vashishta et al., 1999; Zbib and Rubia, 2002a; Zbib et al., 2002b) provide detailed information on deformation, dislocation microstructures, and the dynamics of individual dislocations in pure and alloyed metals. However, the overall complexity and the collective nature of dislocation motion during the deformation process (El-Azab, 2000) is such that it has not been possible to make detailed predictions of plastic deformation in single- or polycrystalline materials. Nor is it possible with present understanding to design from first principles new materials with specific mechanical or deformation properties. Theoretical models and constitutive equations provide critically needed guidance within the realm of known materials and investigated systems, but the development of a fundamental understanding and a comprehensive computational framework for specific and reliable predictions outside known envelopes remains work in progress. The development of an understanding sufficient for direct specification and engineering of materials with new and improved physical properties is a longstanding goal of enormous technological and basic materials science interest.

The effects of grain boundaries, triple-junctions, and chemical constituents on deformation microstructure, dislocation patterning, and mechanical properties are difficult to quantify because of the extended length of dislocations, the long-range of the interactions, and their interactions with structural inhomogeneities result in highly collective, temporally discontinuous dislocation transport (Hähner and Zaiser, 1997; El-Azab, 2000). Accordingly, detailed non-destructive deformation information is needed that covers the mesoscopic length scales (tenths-to-hundreds of microns) of dislocation patterning and the grain-sizes of polycrystalline materials in addition to presently existing information on microscopic and macroscopic length scales. Electron backscattering orientation imaging microscopy (OIM) provides detailed structure grain orientation information with ~ 1 μm spatial resolution on the surfaces of materials (Field, 1997; Sun et al., 2000); however, until recently (Larson et al., 2002), non-destructive, point to point, three-dimensional structure and microstructure measurements with the needed micron resolution have not been available for bulk materials (Poulsen et al., 2001; Lauridsen et al., 2001; Poulsen and Jenson, 2002). X-ray microbeam techniques using synchrotron X-ray sources have now been

developed that provide non-destructive structure, orientation, and strain tensors in single-crystal, polycrystalline, composite, functionally graded, and deformed materials with micron resolution in three-dimensions (Larson et al., 2002; Yang et al., 2003). In the present paper, we describe the salient features of this new X-ray microbeam technique and illustrate its capabilities through measurements of the deformation microstructure in single-crystal and grain-boundary regions of an Al (0.2 wt.% Mg) tri-crystal deformed 20% in plane-strain. The ability of this new technique to generate intra- and inter-granular spatially resolved pole-figures with micron resolution in three-dimensions and angular resolution of a few hundreths of a degree are demonstrated and discussed in relation to plastic deformation investigations. Spatially resolved pole-figure measurements of deformation (local orientation) microstructure near-to and remote-from a grain-boundary are considered in relation to previous OIM measurements and finite-element deformation analyses performed on this sample (Weiland and Becker, 1999).

2. Experiment

The differential-aperture X-ray microscopy (DAXM) technique has been described previously (Larson et al., 2002; Yang et al., 2003). However, the aspects of the 3-D measurement process important for understanding the results and the capabilities of the technique will be outlined. Fig. 1 is a schematic picture of the X-ray microbeam instrument geometry. A polychromatic (white) X-ray beam (such as available on the MHATT-CAT undulator line on Sector 7 and the UNI-CAT-II undulator line on Sector 34 at the Advanced Photon Source (APS) at Argonne

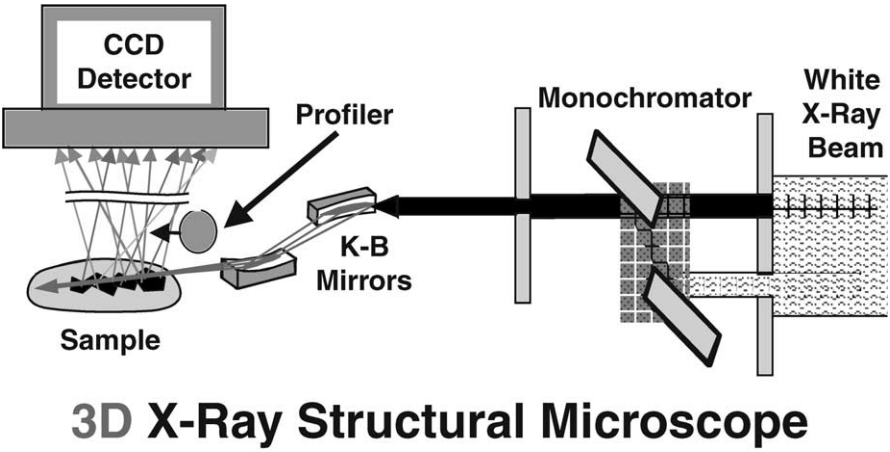

Fig. 1. Schematic of the X-ray structural microscope configuration showing the polychromatic (white) undulator beam incident from the right and passed as a white beam or monochromated by an insertable/removeable scanning monochromator. The white (or monochromatic) beam is then focused by K–B mirrors to ~0.5 μm at the sample position. Laue diffraction patterns are collected by the CCD detector and the diffracted beams are depth profiled using a 50 μm Pt wire.

National Laboratory) is depicted entering from the right. The microbeam facility illustrated has the capability of passing white radiation to the crossed Kirkpatric–Baez (K–B) focusing mirrors. In addition, by inserting a scanning double crystal monochromator, it is possible to pass monochromatic X-rays to the K–B mirrors. Therefore, it is possible to focus either monochromatic or white X-rays onto the sample. The high-precision, elliptically-figured K–B mirrors on the UNI-CAT beamline provide a ~0.5 μm diameter X-ray beam with an ~0.5 millimeter depth of field at the sample position (Ice et al., 2000). The achromatic nature of the totally reflecting K–B mirrors makes it possible to focus all wavelengths of the white beam at the same position. White radiation is a key aspect of the DAXM technique; white X-rays provide full Laue diffraction patterns from each grain irradiated by the beam without rotation of the sample. Moreover, and very importantly, full white-beam diffraction patterns are generated by each segment within each grain irradiated by the X-ray microbeam so that both intra- and inter-granular structural information is available with micron resolution in 3-D.

As indicated in Fig. 1, the Laue diffraction patterns from the sample are collected by a charge coupled device (CCD) X-ray area detector. The CCD camera collects Laue diffraction pictures in the same manner as standard Polaroid X-ray back-reflection cameras, however it is linked to computer control, storage, and analysis capabilities (Ice and Larsen, 2000; Tamura et al., 1999, 2002). The ~0.5 μm diameter X-ray beam provides submicron resolution perpendicular to the beam in the sample, but as illustrated in Fig. 1, the diffraction patterns from different depths along the incident beam are completely overlapped on the CCD detector. The superpositioned white beam patterns can in favorable cases be depth ordered by collecting data for a number of vertical translations of the CCD detector and triangulating peak centroids or grain edges back to the beam position (Stock et al., 1995; Larson et al., 2000; Ice and Larsen, 2000). However, even when conditions are favorable, such techniques provide only grain-average, grain-edge, or local diffraction peak information and not point to point spatially resolved intra-granular information. Powerful techniques using high energy, monochromatic focused beams and sample rotation techniques that provide grain average or grain-boundary spatial resolution have been developed for investigations on somewhat larger length scales (Poulsen et al., 2001; Margulies et al., 2001); these techniques have the important advantage of being full-field so they can be applied in real-time in some cases (Lauridsen et al., 2000; Offerman et al., 2002; Poulsen and Jensen, 2002), but so far they do not provide point to point spatially resolved intra-granular measurements.

Depth profiling of diffracted beams using the knife-edge differential-aperture technique not only provides micron depth resolution of the individual diffracted beams, it provides the ability to digitally reconstruct full diffraction patterns from submicron spatial increments along the microbeam. Full white-beam Laue diffraction patterns mean that full diffraction information can be obtained from submicron volumes in three dimensions without rotating the sample; this is a powerful result that provides the ability to investigate a wide range of diffraction sensitive phenomena, as well as determine structure, orientation, and strain tensors with submicron spatial resolution (Larson al., 2002).

It is of course not possible to construct slits with micron or submicron widths that both absorb hard X-rays (i.e. requirement of >10 μm thickness) and are able to pass the $>45^\circ$ angular range (i.e. requirement of <1 μm thickness) needed to image sufficiently large solid-angles of the diffraction patterns. Therefore, the differential-aperture X-ray microscopy (DAXM) knife-edge technique is used to provide both the large angular acceptance and the desired 1 μm spatial resolution in a process analogous to a step-scanned traveling pinhole camera. As illustrated in Fig. 2, by using a 50 μm diameter Pt wire as a profiler and collecting CCD diffraction images after each micron step of the wire profiler, it is possible to determine the origin along the microbeam of each Laue Bragg reflection with high precision and accuracy.

This depth resolution process is a generalization of the knife-edge technique often used with a spatially integrating detector for profiling the spatial width of incident beams. Since, as discussed above, each volume element (or voxel) traversed by a white microbeam excites a full set of Laue Bragg reflections, it is possible by computer analysis and collation to reconstruct the Bragg diffraction pattern from each micron segment along the microbeam. That is, through the use of the procedure illustrated in Fig. 2 of (1) collecting a CCD image at position [a], (2) stepping the wire to position [b], (3) collecting a second CCD image at position [b], and (4) sub-

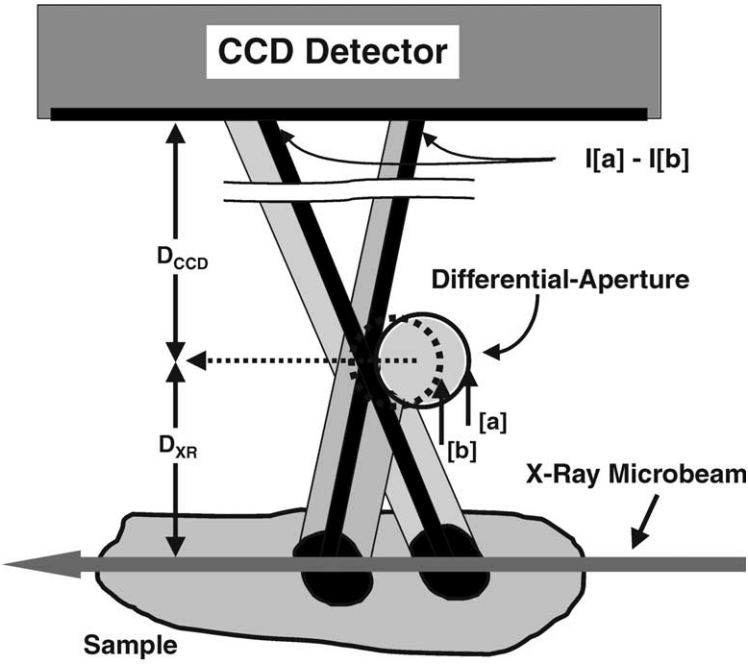

Fig. 2. Illustration of the principle of the DAXM technique for submicron depth profiling showing Bragg diffracted beams from two grains in the sample. The hatched regions of the diffracted beams represent the scattering occluded by moving the profiler from position [a] to position [b]; this intensity is given by the CCD pixel by pixel difference I[a] − I[b]. The source of this differential intensity for each pixel is obtained by triangulating back to the X-ray beam.

tracting the two images (pixel by pixel), the scattering passing through the step distance [a] to [b] can be determined directly. By choosing the distance D_{XR} from the profiling wire to the X-ray microbeam to be much smaller (typically ~100 times smaller) than the distance D_{CCD} to the detector, the origin along the beam of the scattering in each pixel can be determined with submicron resolution by triangulation even with the ~22 μm pixel sizes in our detector. The origin along the beam is found by a linear extrapolation of a line between the pixel position and the wire position down to the position of the microbeam. Repeating this process across the diffracted beams and computer collating the source of the scattering for each reflection transforms the overlapping diffraction patterns into a series of single crystal diffraction patterns; a separate Laue pattern is generated for each micron increment along the penetration depth. These individual diffraction patterns for each submicron voxel along the beam are then available for standard (single-crystal) crystallographic analysis. Of course, if a measurement voxel is centered directly on a grain-boundary, the diffraction pattern for this voxel will contain two superpositioned diffraction patterns that can be handled with built-in multi-grain analysis provisions. The peak intensities for the split-orientation voxel and for the previous and the following single-orientation voxels can be used to apportion the spatial position of the boundary between the two orientations accordingly. Material with submicron grain sizes will have multiple diffraction patterns in each voxel as well, but this situation will not be discussed here.

The analysis of the micron resolution depth resolved diffraction patterns is performed using computer automated techniques developed for crystallographic indexing, orientation, and strain determination of grains in thin film samples (Chung and Ice, 1999; Tamura et al., 1999, 2002; Ice and Larson, 2000; Ice et al., 2002). As outlined in the flow diagram in Fig. 3, digital CCD Laue images are automatically

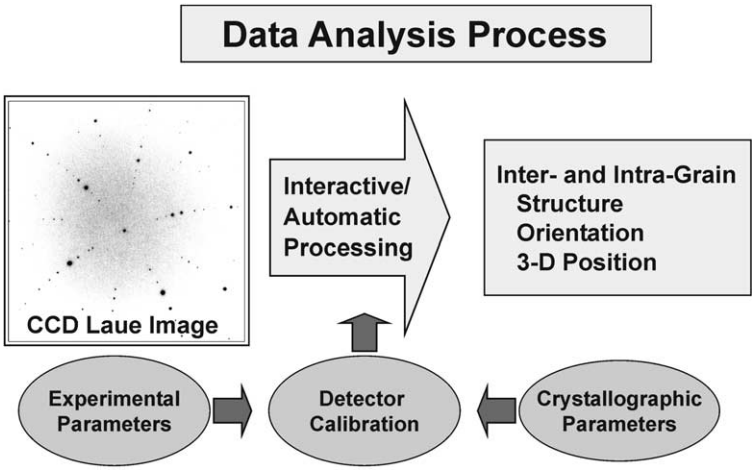

Fig. 3. Schematic view of the data analysis process for spatially resolved Laue diffraction patterns. The system is calibrated using a perfect Si crystal and automatic software indexes the Laue patterns and determines the orientation matrix for the voxel producing the diffraction pattern.

(or interactively) indexed and analyzed to obtain the structure and orientation as a function of depth within the sample. This is handled straightforwardly using a desktop computer after calibration of the various detector angles and distances using Laue images from a Si or Ge crystal standard. The experimental parameters, the known crystallographic properties of the standard calibration crystal, and the structure of the material in the sample to be investigated are input as known data. In principle, the crystal structure of the sample can be treated as a variable to be determined from the spatially resolved diffraction patterns, but this was not done in the present experiment. Determination of elastic strain tensors are handled similarly (Chung and Ice, 1999; Tamura et al., 1999; Larson et al., 2002), but elastic strain is also not to be considered in the present study.

Fig. 4 shows photographs of the Al tri-crystal sample taken before and after deformation. This sample was chosen for study for two reasons. The deformed tri-crystal provides an opportunity to test, demonstrate, and further develop the capabilities of the DAXM technique by measuring deformation microstructure in both single-crystal and grain-boundary regions. Secondly, this sample has been the subject of a previous electron backscattering OIM and finite-element deformation modeling investigation (Weiland and Becker, 1999). The three marked positions in the lower portion of Fig. 4 indicate the position of microbeam measurements made approxi-

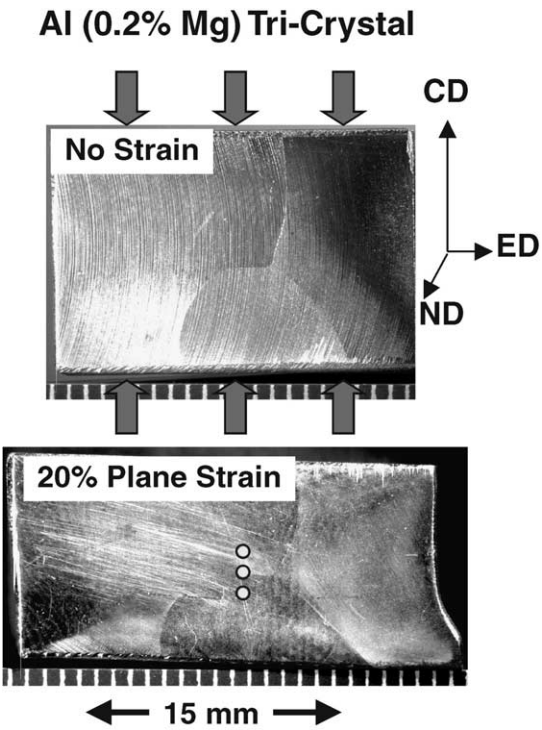

Fig. 4. Photographs of the columnar tri-crystal before and after 20% plane-strain at 200 °C.

mately 1 mm to the left of the triple-junction and 1 mm above and below the grain-boundary as well as at the grain-boundary position. Fig. 5 indicates the microbeam geometry used in the measurements at each of the three positions. As the line drawing in the lower right position in the figure indicates for the case of the measurement at the grain-boundary, the microbeam entered the sample at a 45° angle with the surface and impinged at a 45° angle onto the vertical grain-boundary between the columnar crystal grains. Measurements at these three positions provide an opportunity to assess the impact of a grain-boundary on plane-strain deformation with deformation in single-crystal regions of the same grains.

3. Results

In addition to illustrating the measurement geometry, Fig. 5 shows a depth integrated Laue diffraction pattern (upper left) at the grain-boundary where the microbeam entered the surface of grain-A, passed through the A–B grain boundary, and continued into grain-B. The rather straight vertical streaks in the diffraction pattern are from the (upper) grain-A and the shorter, arc-shaped streaks are from

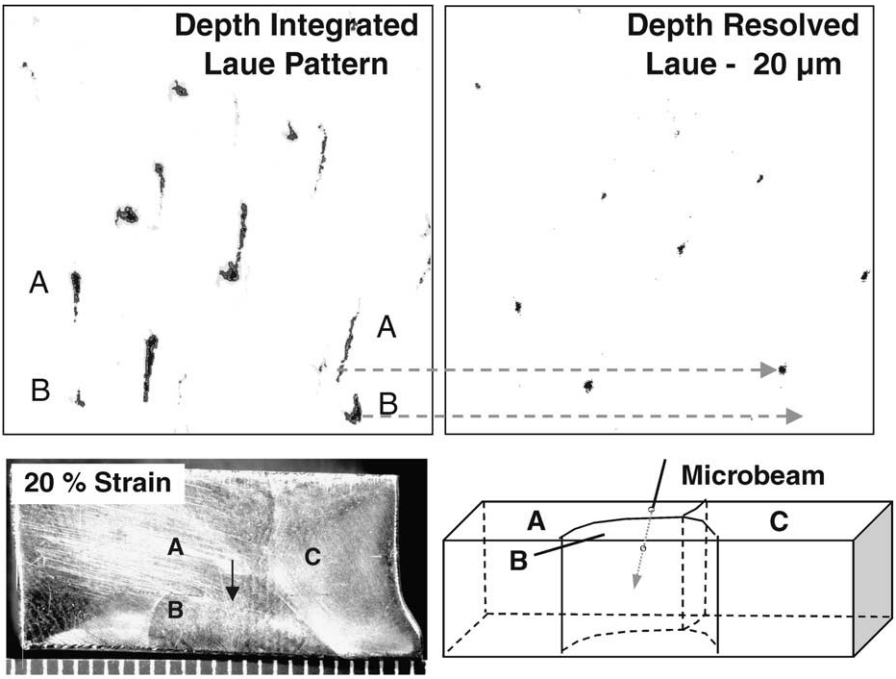

Fig. 5. Depth integrated Laue diffraction pattern showing streaked Bragg spots as the microbeam passes through the A–B grain boundary at 170 μm; the geometry is illustrated in the lower right schematic drawing. The depth resolved Laue pattern is a DAXM reconstructed Laue pattern for the position 20 μm below the surface in grain-A.

grain-B. Since Bragg reflections represent specular scattering from local crystal planes, white-beam Laue diffraction patterns provide a direct mapping of lattice orientation as a function of depth along the microbeam (Barabash et al., 2001). The streaks result from changes in the lattice orientations as a function of depth, and the length of the straight and arc-shaped streaks in Fig. 5 indicate local lattice rotations of more than 7° for the long streaks and only 2–3° for the smaller arc-shaped streaks as the beam penetrates ~250 μm into the crystal. Similar measurements made in the single crystal regions of grain-A and grain-B (discussed below) show diffraction patterns for grain-A or grain-B separately at their respective positions.

The diffraction pattern in the upper right corner of Fig. 5 shows a depth-resolved Laue diffraction image for a depth of 20 μm from the surface along the beam direction in grain-A obtained using the DAXM procedure. The 20 μm position is approximately 150 μm from the A–B grain boundary. This depth resolved Laue diffraction pattern was discussed in the previous section. A dashed arrow indicates the point on the depth integrated Laue image (upper left) corresponding to diffraction from the 20 μm depth. In the depth resolved image, there is of course no evidence of intensity at the position of the grain-B reflections, nor is there intensity from other depths (i.e. other parts of the diffraction streak) of grain-A. Therefore, Fig. 5 illustrates directly the reconstructed (micron spatial resolution) diffraction data from which the orientation of the crystal at a depth 20 μm along the beam is determined by the computer indexing and crystallographic orientation software (Ice, 2000b; Tamura, 1999; Chung, 1999)]. The local orientation change as a function of depth along the entire beam is then found by analyzing analogous images for each position along the penetration depth of the microbeam. The results of such an analysis were combined to obtain the (111), (001), and (110) pole figures in Fig. 6, in which the ~16° angular rotation between grain-A and grain-B is evident as is the range of local crystallographic orientations along the beam. These depth dependent pole figures correspond to a total distance of 275 μm along the microbeam, in which the grain-boundary occurs at the 170 μm point.

Fig. 7 provides an expanded view of the (111) depth-resolved pole figure data in Fig. 6 and, in addition, it includes the depth resolved pole figures for measurements made 1 mm away from the grain boundary. The open squares (i.e. light) markers correspond to measurements made in the single-crystal regions of grain-A and grain-B, while the solid (i.e. dark) circles correspond to measurements made at the A–B grain-boundary position. It is clear from the pole figures that the deformation pattern at the grain-boundary is significantly different from the deformation patterns 1 mm away from the boundary. The surface (S) and grain boundary (G-B) positions are indicated in the expanded views of the individual $<111>$ poles. The polar and meridial grid lines in each of the expanded boxes in Fig. 7 correspond to 5° increments in the polar and meridial angles.

The deformation induced lattice rotations in the single crystal regions fluctuate in the range of 2–5°, while the rotations in the grain-boundary region appear to follow a meandering, but somewhat less fluctuating path, with 5–8° of total rotation. Fig. 8 shows a plot of the total rotation angles measured at all three positions along with plots of the rotation angles resolved about the axis of the plane-strain extension

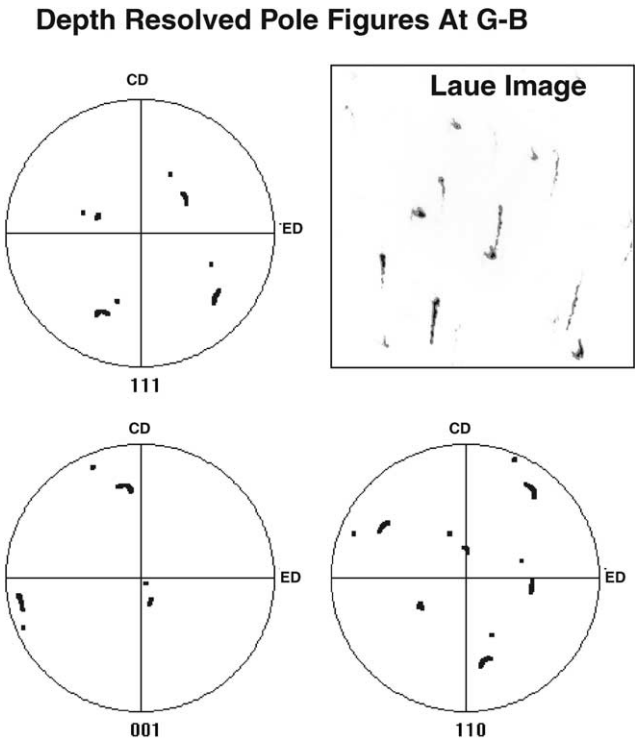

Fig. 6. Depth resolved pole-figures at the A–B grain-boundary corresponding to 275 μm along the microbeam.

direction (ED). Over the first ~100 μm, both the single-crystal and grain-boundary regions of grain-A have ~3.5° rotations around the ED axis, while grain-B has a smaller, more irregular rotation that corresponds to a net rotation of only ~1.5° by a depth of 155 μm. However, from the 100 μm position to the grain-boundary position at 170 μm, the rotations in grain-A increase in magnitude and depart markedly from the ED axis of rotation, while the single crystal region of grain-A continues to rotate around the ED axis.

Making use of the full orientation matrix information that is generated for each micron position along the microbeam and using a coordinate system defined in Fig. 4 by [ED CD TD] where ED is the (horizontal) extension direction, CD is the (vertical) compression direction, and TD is the constrained direction normal to the sample (i.e. transverse direction (TD) in rolling), it is possible to analyze the above observations quantitatively. The single-crystal region of grain-A has a rotation of 3.5° around the [9.1, 3.2, −2.7] axis in going from the surface to 100 μm, it has a 1.0° rotation around the [9.7, 1.9 −1.1] axis from 100 to 189 μm, and the overall surface to 189 μm depth rotation is approximately 4.5° around the [9.3, 2.9, −2.3] axis. Thus the rotations along the beam penetration direction in grain-A have a strong projec-

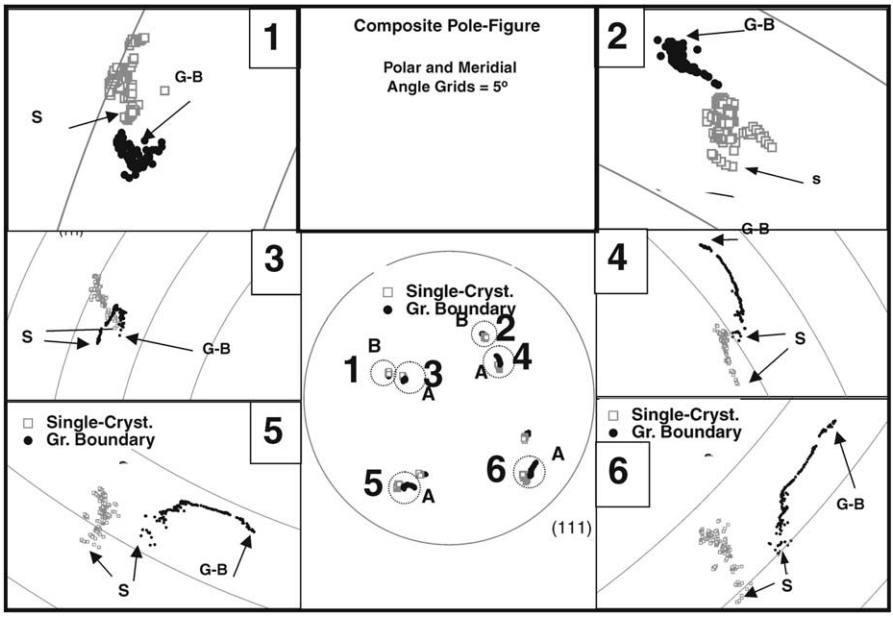

Fig. 7. Expanded view of a composite (111) spatially-resolved pole-figure; measurements at single-crystal positions of grain-A and grain-B and at the grain-boundary position. The dark solid markers denote pole-figures at the A–B grain-boundary; the open squares denote pole figures from the single crystal positions in grain-A and grain-B. The marker S denotes the orientation at the surface position and marker G-B denotes the orientation at the grain-boundary position.

tion around the [ED 0 0] axis for all depths, as suggested in Fig. 8. At the grain boundary position, grain-A has a 3.6° rotation around the [9.4, −0.4, −3.4] axis from the surface to the 100 μm position that is similar to the single-crystal position of grain-A. However, for the 100–170 μm depth immediately adjacent to the grain-boundary, the rotation in grain-A is 4.7° around the [0.2, 0.2, −10.0]; this corresponds to a rotation around the [0, 0, TD] sample normal direction. The overall rotation from the surface to 170 μm corresponds to 6.9° around the [5.1, 0.1 −8.6] axis. The single-crystal position in grain-B has a net rotation of only 1.1° from the surface to 155 μm with a rotation axis of [9.0, 0.9, 4.2]. Because of the relatively small total rotation and the oscillating nature of the rotations, the overall rotation of 1.7° from the surface to 183 μm has a rotation axis of [6.6 ,0.7, 7.5]. These results are summarized in terms of Euler angles in Table 1.

Fig. 9 is a micron resolution misorientation plot obtained by calculating the smallest rotation angle between successive micron positions along the beam direction, where the sign of the rotation was determined by the sense of the rotation axis along the ED axis. There are a few large rotations and a rather larger number of smaller rotations of ∼0.1–0.2° per micron step. Considering that DAXM measurements determine orientations with a precision of ∼0.02°, rotations in the 0.1–0.2° range can be expected to be accurate and not the result of statistical fluctuations and measurement uncertain-

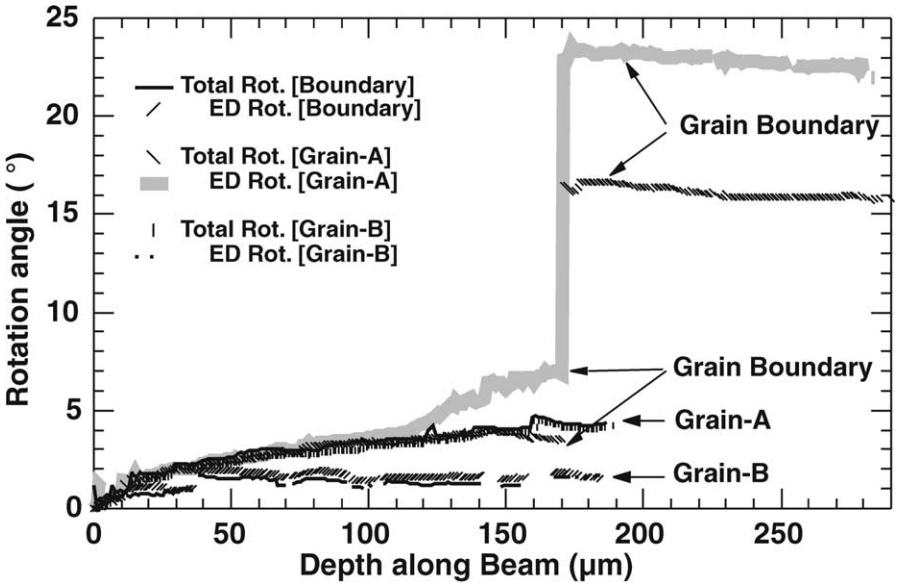

Fig. 8. Total rotation angles and the projection of total rotation angles on the ED axis referenced to the orientation of the first point at the surface of the scan.

ties. The larger number and extended intervals of positive misorientations in grain-A, both in the single-crystal and grain-boundary positions, is a reflection of the deformation induced net curvature around the ED axis observed for grain-A in Fig. 8.

One of the important aspects of the local orientation information is that it provides a direct method for determining the geometrically necessary dislocation

Table 1
Euler angles corresponding to local orientations at specified depth positions in grain A, grain B and at the A/B grain boundary

Grain	Depth (μm)	Euler angles (°)		
		φ_1	Φ	φ_2
A	0	12.65	24.41	−8.44
	100	12.68	21.07	−7.46
	189	12.88	20.03	−7.55
A/B	0	19.89	23.25	−12.00
	100	24.71	20.16	−15.86
	170	29.32	20.02	−15.78
	171	53.73	6.15	−31.05
	250	49.39	6.54	−26.79
B	0	32.20	7.21	−13.60
	155	37.31	5.69	−18.22
	183	36.63	5.67	−18.27

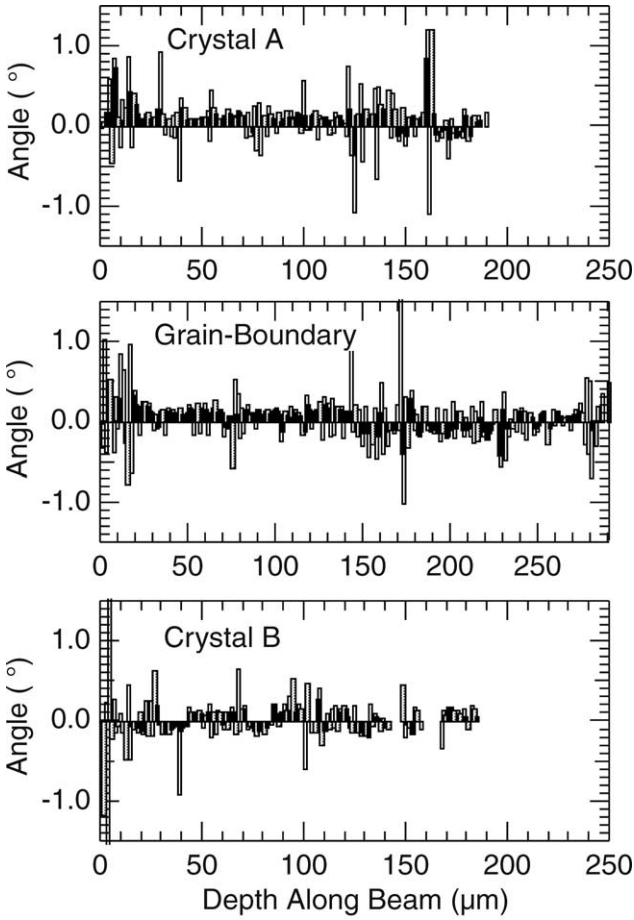

Fig. 9. Misorientation angle per micron along the X-ray microbeam.

(GND) density and the dislocation tensor as a function of depth (Sun et al., 2000; Arsenlis and Parks et al., 1999; El-Azab, 2000). To obtain full GND densities, it is necessary to have a 2D array of line scans so that orientation gradients in all three dimensions can be used to calculate the local dislocation tensor. Although quantitative GND densities are not considered in this paper; we have performed a 4×4 array of lines scans at the A–B grain boundary in order to investigate the lateral dependence of the deformation. The array covered a 9×9 μm^2 area in which 3 μm lateral steps were taken and 1 μm depth resolution was obtained along the beam direction. Fig. 10 shows the geometry for a 1×4 horizontal slice of the 4×4 array of measurements at the A–B grain boundary; it also shows a shaded (false-color) surface plot of the local orientations for the 1×4 slice. The $\sim 7^\circ$ rotations near the boundary in grain-A (Figs. 7 and 8) can be seen to persist laterally, and there is evidence for local patterning in the form of local undulations in the rotations as a

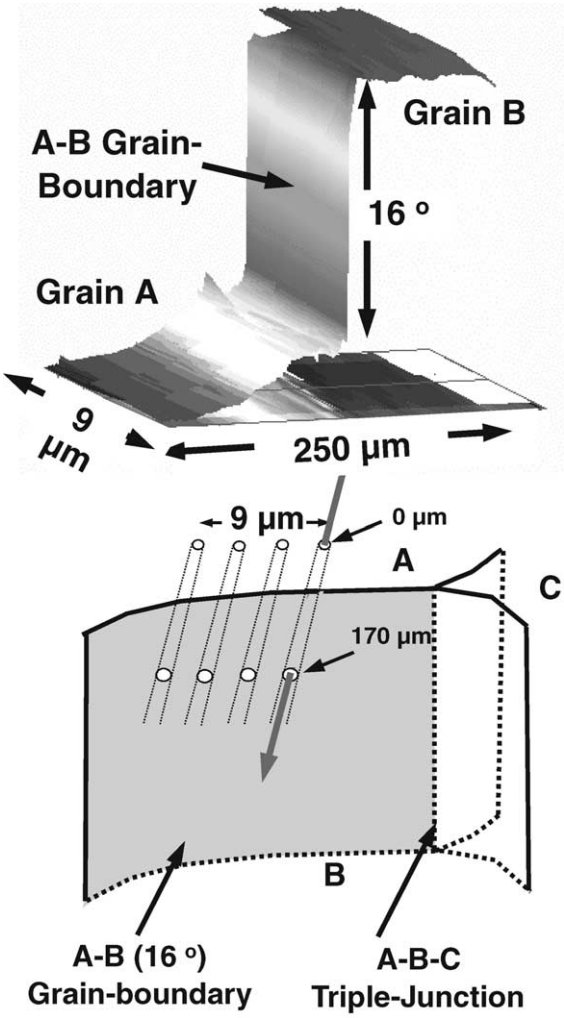

Fig. 10. False-color surface plot of total rotation angle as a function of depth for a 9 μm horizontal slice.

function of depth along the microbeam direction. Taking into consideration the disparity in the length scales in Fig. 10 (i.e. the 9 μm lateral by 250 μm depth dimension), the rotational patterning close to the grain-boundary makes an angle $\sim 45^{\circ}$ with the beam penetration direction. Also, examination of the precise depth of the grain boundary position suggests that the grain boundary may be locally serrated, as it also makes an angle $\sim 45^{\circ}$, while on average the grain-boundary is more or less perpendicular to the projected beam direction. Further analysis and wider lateral scan distances are needed to characterize the local interface geometry in detail and to draw conclusions on such aspects.

4. Discussion

The spatially resolved pole-figure measurements and the rotation angle results presented demonstrate the micron resolution 3-D structural microscopy capabilities of the DAXM technique for studying plastic deformation. The combination of white-beam Laue diffraction and non-destructive extraction of full diffraction patterns with micron spatial resolution in all three directions is an ideal tool for the investigation of the complex crystal distortions associated with plastic deformation. Two-dimensional arrays of line scans will make volume distributions of local orientation changes, deformation and evolution possible. Of course, scanning techniques such as this limit the application of real-time measurements, but stop-action techniques can be used to follow evolution in many cases. Single line scans presently require 30–60 min; however, most of the time is CCD detector readout so significant improvements in speed will be realized as detector speed improves. X-ray energies of ~8–22 keV in the present system limit the penetration depths in transition metal and higher Z materials to less than ~40–50 μm, whereas high energy techniques (Poulsen et al., 2001; Lauridsen et al., 2001; Margulies, 2001; Offerman et al., 2002; Poulsen and Jensen, 2002) have larger penetration distances and they have been able to perform grain-average plastic strain and recrystallization in real-time, but so far have not demonstrated point-to-point micron 3-D spatial resolution. Nevertheless, the range of plastic deformation and fundamental microstructural investigations that can be addressed non-destructively in 3-D with micron spatial resolution is extremely wide. Both the high-energy monochromatic and the white-beam Laue X-ray microbeam techniques mentioned are relatively new, advancing rapidly, and can be expected to undergo significant enhancements in both speed and resolution capabilities.

The grains of the columnar tri-crystal would not be expected to deform with strict columnar symmetry. However, the magnitude of the rotation over ~100 μm near the surface observed in the spatially resolved pole-figure results in the single-crystal regions of grain-A and grain-B suggests that the angular rotations may be, at least in part, the result of surface-friction-induced lattice rotations in the plane strain process. The lattice rotations near the surface in grain-A in particular (and in grain-B to a lesser extent) have a strong depth dependence; this is of course an area that requires additional study. Although the measurements in grain-A were performed with the beam traveling at a 45° angle toward the grain-boundary as well as 45° into the sample, the measurements 1 mm away from the A–B grain-boundary remain essentially unchanged for at least half-a-millimeter toward the grain-boundary. Moreover, the measurements made at the A–B grain-boundary position (where the microbeam enters the crystal ~170 μm from the boundary) indicate similar 3–5° rotations about the ED axis for the first 100 μm. This issue will be investigated further by sectioning the sample perpendicular to the normal direction so that the center of the crystal is accessible for both OIM and X-ray microbeam characterization and comparison with the finite element modeling (Weiland and Becker, 1999). Measurements without the potential for extrinsic surface issues will provide more reliable microstructure information and the possibility of relating to recent in situ microbeam X-ray deformation results reported by Margulies et al. (2001).

Despite what appears to be the presence of friction effects superposed on the plane-strain deformation microstructure, it is clear from the depth dependent pole-figure measurements that the deformation near the grain-boundary is significantly different from that in the single crystal regions remote from the boundary. This effect is indicated in particular by the fact that a rotation around the TD axis dominated the deformation in the last 70 μm, i.e. from the 100 μm position to the grain boundary located at 170 μm. In general, the deformation in grain-B produced a smaller total rotation than that observed in grain-A; however, the local accordion-like rotations in Fig. 9 are similar for grain-B and grain-A.

5. Conclusion

X-ray microbeam techniques for performing micron resolution, spatially resolved pole-figure measurements have been discussed and capabilities for studying local orientations and plastic deformation using this technique have been demonstrated. The results showed that micron resolution plastic deformation measurements could be performed directly up to and through a large-angle grain-boundary. Significant differences were observed in the deformation microstructure near a grain-boundary in the plane-strained columnar tri-crystal, as compared to single-crystal regions, and evidence for friction-induced near-surface rotations was found.

Acknowledgements

The measurements were performed on the MHATT-CAT and UNI-CAT beam lines at the Advanced Photon Source (APS); the APS is supported by the US Department of Energy, Office of Science. This research was sponsored by the US Department of Energy Basic Energy Sciences, Division of Materials Sciences under contract with Oak Ridge National Laboratory, managed by UT-Battelle, LLC.

References

Adams, B.L., Wright, S.I., Kunze, K., 1993. Orientation imaging: the emergence of a new microscopy. Metall. Trans. A 24, 819–831.

Arsenlis, A., Parks, D.M., 1999. Crystallographic aspects of geometrically necessary and statistically stored dislocation density. Acta Mater. 47, 1597–1611.

Barabash, R., Ice, G.E., Larson, B.C., Pharr, G.M., Chung, K.-S., Yang, W., 2001. White microbeam diffraction from distorted crystals. Appl. Phys. Lett. 79, 749–751.

Bertram, A., Böhlke, Th., Kraska, M., 1997. Numerical simulation of deformation induced anisotropy of polycrystals. Computational Materials Science 9, 158–167.

Bulatov, V., Abraham, F.F., Kubin, L., Devincre, B., Yip, S., 1998. Connecting atomistic and mesoscale simulations of crystal plasticity. Nature 391, 669–672. (1998).

Chung, J.-S., Ice, G.E., 1999. Automated indexing for texture and strain measurement with broad-band-pass X-ray microbeams. J. Appl. Phys. 86, 5249–5255.

Cleri, F., Yip, S., Wolf, D., Phillpot, S.R., 1997. Atomic-scale mechanism of crack-tip plasticity: dislocation nucleation and crack-tip shielding. Phys. Rev. Lett. 79, 1309–1312.

Devincre, B., Kubin, L.P., Lemarchand, C., Madec, R., 2001. Mesoscopic simulations of plastic deformation. Mater. Sci. Eng. A309-A310, 211–219.

El-Azab, A., 2000. Statistical Mechanics treatment of the evolution of dislocation distributions in single crystals. Phys. Rev. B 61, 11956–11966.

Field, D., 1997. Recent advances in the application of orientation imaging. Ultramicroscopy 67, 1–9.

Fleck, N.A., Hutchinson, J.W., 1997. Strain-gradient plasticity. Advances in Applied Mechanics 33, 295–361.

Gao, H., Huang, Y., Nix, W.D., 1999. Modeling plasticity at the micrometer scale. Naturwissenschaften 86, 507–515.

Hähner, P., Zaiser, M., 1997. From mesoscopic heterogeneity of slip to macroscopoic fluctuations of stress and strain. Acta Mater. 45, 1067–1075.

Hansen, N., Huang, X., 1998. Microstructure and flow stress of polycrystals and single crystals. Acta Mater. 46, 1827–1836.

Hansen, N., Huang, X., Hughes, D.A., 2001. Microstructural evolution and hardening parameters. Mater. Sci. Eng. A317, 3–11.

Hirsch, P.B., Roberts, S.G., 1995. Comment on the brittle-to-ductile transition: a cooperative dislocation generation instability; dislocation dynamics and the strain-rate dependence of the transition temperature. Acta Mater. 44, 2361–2371.

Hughes, D.A., Hansen, N., 1997. High angle boundaries formed by grain subdivision mechanisms. Acta Mater. 45, 3871–3886.

Huang, Y., Xue, Z., Gao, H., Nix, W.D., Xia, Z.C., 2000. A study of microindentation hardness tests by mechanism-based strain gradient plasticity. J. Mater. Res. 15, 1786–1796.

Ice, G.E., Chung, J.-S., Tischler, J.Z., Lunt, A., Assoufid, L., 2000. Elliptical x-ray microprobe mirrors by differential deposition. Rev. Sci. Instrum. 71, 2635.

Ice, G.E., Larson, B.C., 2000. 3D x-ray crystal microscope. Adv. Eng. Mater. 2, 643–646.

Kubin, L., Devincre, B., Tang, M., 1998. Mesoscopic modeling and simulation of plasticity in fcc and bcc crystals: dislocation intersections and mobility. J. Comput.-Aided Mater. Des 5, 31–54.

Larson, B.C., Tamura, N., Chung, J.-S., Ice, G.E., Budai, J.D., Tischler, J.Z., Yang, W., Weiland, H., Lowe, W.P., 2000. 3D measurement of deformation microstructure in Al(0.2%)Mg using submicron resolution white x-ray microbeams. Mat. Res. Soc. Symp 590, 247–252.

Larson, B.C., Yang, W., Ice, G.E., Budai, J.D., Tischler, J.Z., 2002. Three-dimensional x-ray structural microscopy with submicrometre resolution. Nature 415, 887–890.

Lauridsen, E.M., Juul Jensen, D., Poulsen, H.F., Leinert, U., 2000. Kinetics of individual grains during recrystallization. Scripta Mater. 43, 561–566.

Lauridsen, E.M., Schmidt, S., Suter, R.M., Poulsen, H.F., 2001. Tracking: a method for structural characterization of grains in powders or polycrystals. J. Appl. Cryst 34, 744–750.

Lassen, K., 1996. Automatic localisation of electron backscattering pattern bands from Hough transform. Mater. Sci. Technol. 12, 837–843.

Liu, Q., 1995. A simple and rapid method for determining orientations and misorientations of crystalline specimens in TEM. Ultramicroscopy 60, 81–89.

Lopes, A.B., Barlat, F., Gracio, J.J., Ferreira Duarte, J.F., Rauch, E.F., 2003. Effect of texture and microstructure on strain hardening anisotropy for aluminum deformed in uniaxial tension and simple shear. Int. J. Plasticity 19, 1–22.

Margulies, L., Winther, G., Poulsen, H.F., 2001. In situ measurement of grain rotation during deformation of polycrystals. Science 292, 2392–2394.

Maudlin, P.J., Bingert, J.F., Gray, G.T., 2003. Low-symmetry plastic deformation in BCC tantalum: experimental observations, modeling and simulations. Int. J. Plasticity 19, 483–515.

Nakamachi, E., Xie, C.L., Morimoto, H., Morita, K., Yokoyama, N., 2002. Formability assessment of FCC aluminum alloy sheet by using elastic/crystalline viscoplastic finite element analysis. Int. J. Plasticity 18, 617–632.

Needleman, A., 2000. Computational mechanics at the mesoscale. Acta Mater. 48, 105–124.

Offerman, S.E., van Dijk, N.H., Sietsma, J., Grigull, S., Lauridsen, E.M., Margulies, L., Poulsen, H.F., Rekveldt, M.T., van der Zwaag, S., 2002. Grain nucleation and growth during phase transformations. Science 298, 1003–1005.

Panchanadeeswaran, S., Doherty, R.D., Becker, R., 1996. Direct observation of orientation change by channel die compression of polycrystalline aluminum—use of a split sample. Acta Mater. 44, 1233–1262.

Poulsen, H.F., Nielsen, S.F., Lauridsen, E.M., Schmidt, S., Suter, R.M., Lienert, U., Margulies, L., Lorentzen, T., Juul Jensen, D., 2001. Three-dimensional maps of grain boundaries and the stress state of individual grains in polycrystals and powders. J. Appl. Cryst 34, 751–756.

Poulsen, H.F., Jensen, D.J., 2002. From 2D to 3D microtexture investigations. Materials Science Forum 408, 49–66.

Radhakrishnan, B., Sarma, G.B., Zacharia, T., 1998. Modeling the kinetics and microstructural evolution during static recrystallization— monte carlo simulation of recrystallization. Acta Mater. 46, 4415–4433.

Richmond, O., Alexandrov, S., 2000. Nonsteady planar ideal plastic flow: general and special analytical solutions. J. Mech. Phys. Sol 48, 1735.

Stock, S.R., Guvenilir, A., Piotrowski, D.P., Rek, Z.U., 1995. High resolution synchrotron x-ray diffraction tomography of polycrstalline samples. Mater. Res. Soc. Proc 375, 275–280.

Sun, S., Adams, B.L., King, W.E., 2000. Observations of lattice curvature near the interface of a deformed aluminum bicrystal. Philos. Mag. A 80, 9–25.

Tamura, N., Chung, J.-S., Ice, G.E., Larson, B.C., Budai, J.D., Tischler, J.Z., Yoon, M., 1999. Strain and texture in Al-interconnect wires measured by x-ray microbeam diffraction. Mater. Res. Soc. Proc 563, 175–180.

Tamura, N., MacDowell, A.A., Celestre, R.S., Padmore, H.A., Valek, B., Bravman, J.C., Spolenak, R., Brown, W.L., Marieb, T., Fujimoto, H., Batterman, B.W., Patel, J.R., 2002. High spatial resolution grain orientation and strain mapping in thin films using polychromatic submicron x-ray diffraction. Appl. Phys. Lett. 80, 3724–3726.

Vashishta, P., Kalia, R.K., Nakano, A., 1999. Large-scale atomistic simulations of dynamic fracture. Computing in Science and Engineering 1, 56–65.

Weiland, H. and Becker, R. 1999. Analysis of mesoscale deformation structures in aluminum. In: Leffer, T., Pederson, A. P. (Eds.), Proceedings of 20th Risø Int. Symp. on Mater. Sci. Deformation-Induced Microstructures: Analysis and Relation to Properties, p. 213.

Yang, W., Larson, B.C., Ice, G.E., Tischler, J.Z., Budai, J.D., Chung, K.-S., Lowe, W.P., 2003. Spatially resolved Poisson strain and anticlastic curvature measurements in Si under large deflection bending. Appl. Phys. Lett. 82, 3856–3858.

Zbib, H.M., de la Rubia, T.D., 2002a. A multiscale model of plasticity. Int. J. Plasticity 18, 1133–1163.

Zbib, H.M., de la Rubia, T.D., Bulatov, V., 2002. A multiscale model of plasticity based on discrete dislocation dynamics. J. Eng. Mater. Technol 124, 78–87.